EUROPEAN ORGANIZATION FOR NUCLEAR RESEARCH

π^-p AND K^-p ELASTIC SCATTERING AT 6.2 GeV/c

T. Buran[1], Å. Eide[2,3], P. Helgaker[1], P. Lehmann, A. Lundby, A. Navarro-Savoy, L. Staurset[1] and O. Sørum[1]

CERN, Geneva, Switzerland

C. Baglin, P. Briandet, P. Fleury, G. de Rosny and J.M. Thenard

Ecole Polytechnique, Paris, France

P.J. Carlson and K.E. Johansson

University of Stockholm, Stockholm, Sweden

B. d'Almagne, F. Richard and D. Treille

Laboratoire de l'Accélérateur Linéaire, Orsay, France

V. Gracco

University of Genova and INFN, Genova, Italy

ABSTRACT

Data on 6.2 GeV/c π^-p and K^-p elastic scattering cross-sections are presented in the range $0.3 < -t < 10.7$ $(GeV/c)^2$.

Large-angle π^-p scattering differential cross-sections oscillate around an average differential cross-section of 50 nb/$(GeV/c)^2$, with minima at $\cos\theta_{cm} \approx 0$ and -0.4. The well-known dip at $-t = 2.8$ $(GeV/c)^2$ remains constant in t. In the backward direction there is a dip at $-u \approx 1$ $(GeV/c)^2$.

K^-p elastic scattering has a diffraction peak with a slope of 7.30 ± 0.08 $(GeV/c)^{-2}$ in the region $0.3 < -t < 0.6$ $(GeV/c)^2$. The structure at about $-t = 1$ $(GeV/c)^2$ is less pronounced than at 5 GeV/c. The large-angle region is characterized by a very fast decrease of the differential cross-section with increasing energy.

Geneva - 7 April 1976

(Submitted to Nuclear Physics B)

---

1) Present address: Department of Physics, University of Oslo, Oslo 3, Norway.

2) Present address: Agder Regional College, Box 607, N-4601 Kristiansand, Norway.

3) Supported in part by Ecole Polytechnique, Paris, France.

1. INTRODUCTION

We present the results of measurements of π^-p and K^-p elastic scattering at an incident momentum of 6.2 GeV/c. The experiment was performed at the CERN Proton Synchrotron (PS). We have earlier reported results of $\pi^\pm p$, $K^\pm p$, and $\bar{p}p$ elastic scattering at 5 GeV/c [1], π^+p [2,3], and K^+p [3,4] large-angle scattering at 10 GeV/c, and $\bar{p}p$ elastic scattering at 6.2 GeV/c [5].

Elastic scattering of π^- on protons has been studied in the forward region up to an energy of 200 GeV/c. In the region $0.1 < -t < 1.0$ $(GeV/c)^2$, no structure has been observed in the energy range from 2 to 200 GeV/c [6-13]. Dips have been observed at $-t = 1.2$ and 2.8 $(GeV/c)^2$. The first[14-19] changes into a break at about 4 GeV/c [16,17,20-24]. The second dip[16,17,20] remains at 13.8 GeV/c [20] but has changed into a shoulder at 22.6 GeV/c [20]. This region of t has not been measured above 22.6 GeV/c. The structures seem to remain fixed in t.

In the 90° c.m. elastic scattering region, a high statistics experiment at 5 GeV/c [1] reports structures in the differential cross-sections with dips at $-t = 4.5$ and 5.8 $(GeV/c)^2$ corresponding to $\cos\theta \approx 0$ and -0.35, respectively. The only other experiment at high energy [9.8 GeV/c [22]] covering this angular region has not sufficient statistics to give information on structures.

The backward region has been studied up to 16 GeV/c [16,22,25-34]. For -u approaching 0 there is a sharp rise in cross-section for energies above 3 GeV/c. The dip at $-u \approx 1$ $(GeV/c)^2$ which shows up at 3 GeV/c remains at this u-value at 3.5 GeV/c [16,29]. At 10 GeV/c it has developed into a break[22]. This structure may therefore be of the same nature as the structures at $-t \approx 1.2$ and 2.8 $(GeV/c)^2$.

Several mechanisms, such as diffraction and t-channel Regge-pole exchanges[35], have been evoked in order to explain the forward elastic scattering. Backward scattering has been explained in terms of direct channel resonances[36] or the exchange of Reggeized baryon trajectories[37]. In the large angular region, several models have been proposed. One of the most successful has been the constituent interchange model[38-40], which predicts an energy dependence equal to s^{-8} (around 90° c.m.). They make no predictions about structures in this region.

The K^-p elastic scattering has been well studied in the forward direction up to 100 GeV/c [41]. For $-t < 0.8$ $(GeV/c)^2$, however, only a limited number of experiments have been performed in the momentum range 3 to 14 GeV/c [1,6,7,41-52].

The structure at about $-t = 1$ $(GeV/c)^2$ is well studied at lower energies. At 3.6 GeV/c there is a pronounced dip followed by a secondary maximum at this value of t [42]. With increasing energy, this develops into a shoulder. For higher energies there are indications[22,44] that the structure gets steadily less pronounced with increasing energy.

Owing to the very small differential cross-sections, very few measurements have been reported for $-t > 3$ (GeV/c)^2 [1,22,42,48] at high energies. The differential cross-section is known to decrease quickly with energy. Recently much attention has been given to scattering around 90° c.m. Models involving the exchange of constituents[38-40] have predicted energy dependence like s^{-8} for 90° c.m. scattering.

In the course of our experimental program we have earlier reported[1] the discovery of a backward peak in K^-p elastic scattering at 5 GeV/c. The energy variation of the differential cross-section in the backward direction could be used to test different models for the exchange[53].

2. APPARATUS AND DATA ANALYSIS

The experimental set-up was of a spectrometer type, using spark chambers and proportional chambers for trajectory determination. A spectrometer magnet was used to momentum-analyse the forward-going particle. The layout is schematically shown in Fig. 1. The inelastic events were filtered out during the off-line data analysis on the basis of cuts on kinematical variables alone, with no additional fitting procedure. For details of the apparatus and the data analysis we refer to Ref. 5.

2.1 π^-p elastic scattering

The incident beam contained approximately 1.1% $\bar{p}$, 1.4% K^-, and 97.5% π^- and μ^-. For target 1 no triggering on π^- events were generally accepted in order to favour K^- and $\bar{p}$ events. However, one short run was made with π^- accepted in target 1. This provided data in the t-range 1.5 to 2.5 (GeV/c)^2 and 9.4 to 10.7 (GeV/c)^2. In order to suppress triggering on π^-p events from target 2, an additional dead-time was imposed. This had a length of 100 ms and acted on the π^-p trigger only. During a short run with lower intensity of the incident beam, data were taken without the suppression of π^-p events. The data from target 2 covered the t-interval $1.7 < -t < 9.5$ (GeV/c)^2 and thus overlapped with the data from target 1.

The two samples of data from target 2 were analysed separately. The normalization of the data, for which the additional dead-time was imposed, was obtained in the region $1.5 < -t < 2.2$ (GeV/c)^2 where the cross-section was large enough to provide good statistics. This normalization factor, obtained from the 7 t-bins in this region, was 4.41 ± 0.13.

As for the $\bar{p}p$ analysis (Ref. 5), an over-all correction factor was included. A normalization factor of 1.3 for target 2 data relative to the target 1 data was obtained. Finally, an over-all factor of 1.7 was used for the combined data.

The background of non-elastic events was examined in different t-regions, by studying the sample of data being just outside the cut-off values of the parameters defining the elastic events. The percentage of the background changed smoothly from about 8% for $|t| \lesssim 2.2$ (GeV/c)^2 to about 30% around $|t| = 2.8$ (GeV/c)^2 and back to about 10% from $|t| \approx 3.2$ (GeV/c)^2 onwards.

The background was subtracted from the raw data before the cross-sections were calculated. The errors in the cross-sections contain errors from this background subtraction together with the errors in adding the dead-time data to the parasitic data for target 2. Finally, the errors from statistics are folded in.

A total number of 64,500 π^-p elastic events was used for the cross-section calculations. Of these, 11,500 events occurred in target 1, 22,000 events in target 2 for the parasitic run, and 31,000 events were taken during the main run with the additional dead-time for the π^-p events.

2.2 K^-p elastic scattering

The procedure of selecting elastic events on the basis of cuts on kinematical variables alone, with no additional fitting procedure, posed no problems in the analysis of the events in the forward regions, i.e. for $-t < 4$ (GeV/c)^2. For the events with a value of $-t > 4$ (GeV/c)^2 the background was too large to provide a significant signal-to-background ratio, and thus only upper limits for the differential cross-section are given in this t-region.

The two bins, $4.5 < -t < 8$ (GeV/c)^2 and $8 < -t < 9.5$ (GeV/c)^2, had five and nine events in target 2, respectively, within the cuts, and with no background correction. For $8 < -t < 9.5$ (GeV/c)^2 we had 10 events in target 1, also with no background correction. We believe that the background in these bins, in addition to inelastic events, consists of elastic π^-p events. This is due to a small inefficiency of the C_2 Čerenkov counter, counting pions. Kinematically the pion events are very similar to the kaon events, particularly for small absolute values of t. Also for large values of t, the kinematical differences are so small that misidentified pion events can fall within the cuts in the kinematical variables.

In the backward region, also the reaction $K^-p \to \Sigma\pi$ could have candidates within the cuts. This possibility was examined by a special Monte Carlo run, using the observed cross-section at 5.47 GeV/c [28,54] estimated to be 3 ± 2 μb in the backward region. With this cross-section we find from our Monte Carlo run that 9 events of the type $K^-p \to \Sigma\pi$ could have passed through our cuts, simulating an elastic K^-p backward scattering. Our original 20 events in the last bin, $9.5 < -t < 10.5$ (GeV/c)^2, were thus reduced to 11 before the upper limit of the cross-section was calculated.

A normalization factor for the data in the forward direction was obtained in the same way as for the antiproton-proton data[5]. Similarly, the overlap region in t, from the two targets, provided the normalization factor for the data in target 2 relative to the data in target 1. This observed difference was consistent with the results the calculations gave. The data from target 2 were a factor of 1.5 lower than those from target 1, which again were to be multiplied by a factor of 1.7 to take into account the non-t-dependent effects which were not included in the Monte Carlo program, giving the t-dependent acceptance for the apparatus.

A total number of 157,300 K^-p elastic events was used for the cross-section calculations. A majority of these, 156,100 events, occurred in target 1, and 1,200 events occurred in target 2. The kinematical region covered by the apparatus was $0.3 < -t < 10.5$ $(GeV/c)^2$, which corresponds to about $19.5° < \theta_{cm} < 170°$. The two targets had an overlap region in t given by $1.4 < -t < 2.5$ $(GeV/c)^2$.

3. RESULTS AND DISCUSSIONS

The elastic differential cross-sections, based on the number of observed events, the acceptance calculations, and the normalization factors, are given in Table 1 for π^-p scattering and in Table 2 for K^-p scattering. The errors are statistical only, based on the number of observed events, the background subtraction, and the Monte Carlo calculation, the last having little significance. We estimate the over-all normalization error to be ±20%.

3.1 π^-p results

Our measured differential cross-sections are shown together with data from other experiments in Figs. 2-5. For $-t < 1.5$ $(GeV/c)^2$ our data agree with those of Owen et al.[22], taking into account normalization errors of the two experiments and also the energy dependence. The recent data of Ambats et al.[55] at 6 GeV/c are significantly higher for $-t < 1.2$ $(GeV/c)^2$. Our K^-p data in the same t-interval do agree with the data of Ambats et al. (see below).

Thanks to the high statistics, our data permit a detailed study of structures over a large angular range. In Fig. 2 the differential cross-sections are displayed as a function of -t, in Figs. 3 and 4 as a function of $\cos \theta_{cm}$, and finally in Fig. 5 the backward region is displayed as a function of u. The structures observed in the angular distribution are shown in Table 3.

The dip for $-t = 2.8$ $(GeV/c)^2$ is clearly a fixed t-structure. This dip has been seen up to an incident momentum of 14 GeV/c [20]. It is interesting that this structure develops differently for π^-p and π^+p [1,3,20].

For scattering in the region around 90° c.m., $0.5 < \cos\theta_{cm} < -0.5$, not much data exist. From our earlier data at 5 GeV/c [1] and from the data of Owen et al.[22] we tentatively conclude that we observe fixed $\cos\theta_{cm}$ structures for $\cos\theta_{cm} = 0$ and $\cos\theta_{cm} = -0.4$.

The parton model of Gunion et al.[38] makes predictions of the s-dependence of the π^-p differential scattering cross-section for this large angular scattering region:

$$\frac{d\sigma}{dt} = \frac{\sigma_0}{s^8} \frac{1+z}{(1-z)^4} \left[4\beta(1+z)^{-2} + \alpha\right]^2 ,$$

with $z = \cos\theta_{cm}$, $\alpha = 2$, $\beta = 1$.

We use $\sigma_0 = 440$ mb $(\text{GeV})^{14}$ so as to make the $\cos\theta_{cm} = 0$ π^+p differential cross-section at 10 GeV/c agree with the measured one, which is 1.6 ± 0.4 nb/$(\text{GeV/c})^2$ [3]. With the same constants we calculate the cross-sections at 5, 6.2, and 10 GeV/c, predicted by the model, in the 90° c.m. scattering region. The results are shown in Fig. 3.

As a general remark, all measured π^-p angular distributions show several structures, not predicted by the model. This is also true for the case of π^-p elastic scattering[3]. The average shape, however, does seem to agree with the model, although the absolute values of the predicted differential cross-sections are lower than the measured ones at 6.2 and 10 GeV/c and higher at 5 GeV/c.

The backward region is explored in detail in Fig. 5, where the differential cross-section is plotted as a function of u. The data shown at 3.5 and 5 GeV/c are both taken from two different experiments (3.5 GeV/c from Refs. 16 and 29, and 5 GeV/c from Refs. 3 and 28). Our data for $-u < 1.3$ $(\text{GeV/c})^2$ come from target 1, hence the low statistics. The data clearly suggest a fixed u-structure for $-u \approx 1$ $(\text{GeV/c})^2$. It seems to become less pronounced with increasing energy, as observed for the two structures in the forward region.

It is interesting to note that this dip for $u \approx -1$ $(\text{GeV/c})^2$ in the backward direction is present in a study of the helicity amplitudes with definite u-channel isospin[56]. The pure I = 3/2 channel shows a very systematic behaviour as far as zero locations of the s-channel helicity flip amplitude are concerned: through the whole phase-shift energy region ($s < 6$ GeV^2) there is a zero for $u \approx -1$ $(\text{GeV/c})^2$, which agrees with what we are observing at 6.2 GeV/c.

3.2 K^-p results

The measured differential cross-sections are shown together with data from other experiments in Figs. 6-9. In Fig. 6 we compare our data for $-t < 1.7$ $(\text{GeV/c})^2$ with the recent data of Ambats et al.[55] at 6.0 GeV/c. The agreement is good, taking into account the normalization errors of the two experiments.

The earlier data of Owen et al.[22] at 5.8 and 5.9 GeV/c extend out to $-t = 5.3$ (GeV/c)^2. These data, statistically less significant, also agree with our data at 6.2 GeV/c.

For $-t < 0.6$ (GeV/c)^2 the K^-p differential cross-section shows an exponential decrease with $-t$. This is demonstrated in Fig. 7 where we have plotted the slope b in the function $A\, e^{bt}$, fitted to the data points in the region 0.31 (GeV/c)$^2 < -t < t_{max}$, t_{max} being in the range $0.41 < -t_{max} < 0.95$ (GeV/c)^2. The corresponding χ^2 probability is also plotted. We obtain a slope parameter $b = 7.30 \pm 0.08$ (GeV/c)^2 in the region $0.3 < -t < 0.6$ (GeV/c)^2, and with a χ^2 probability of 35%. No additional term of the form e^{ct^2} gave any better fit in this t-range, the probability of $c = 0$ being about 39%, obtained from the Fisher test.

The K^-p forward slope seems to be constant around 7.5 (GeV/c)^2 in the range 2-20 GeV/c [57]. Ambats et al.[55], fitting their K^-p data for 3-6 GeV/c in the range $0.05 < -t < 0.44$ (GeV/c)^2, observe no or very little antishrinkage. At 6 GeV/c they get a value of the slope of 7.6 ± 0.1 (GeV/c)^2. Antipov et al.[11], using existing data in the momentum range 5-40 GeV/c, find that for $-t < 0.3$ (GeV/c)^2 the forward peak shrinks, whereas for $-t = 0.4$ (GeV/c)^2 the slope is constant. A compilation[41,57] of fits to the K^-p forward peak over the range $0.07 < -t < 0.3$ (GeV/c)^2 shows a definite shrinkage as the momentum increases from 8 to 100 GeV/c.

The evolution of the dip-bump structure in the angular distribution around $-t = 1.5$ (GeV/c)^2 is shown in Fig. 8. For incident momenta < 5 GeV/c, existing data show a clear dip-bump structure with the dip at around $-t = 1$ (GeV/c)^2 and with a secondary maximum diminishing with increasing momenta[42,45,48]. For incident momenta > 5 GeV/c the secondary maximum develops into a shoulder. From Fig. 8 we notice that this shoulder diminishes further from 5 to 6.2 GeV/c incident momentum. For $-t > 1$ (GeV/c)^2 the differential cross-section decreases quickly with energy (Fig. 8).

In Fig. 9 we show as a function of $\cos\theta_{cm}$ our present data at 6.2 GeV/c together with our earlier data at 5 GeV/c [1] and with the data of Lowman et al.[42] at 3.6 GeV/c. Also shown in this figure is the prediction of the parton model of Gunion et al.[38] at 6 GeV/c.

For K^-p they predict a differential cross-section

$$\frac{d\sigma}{dt} = \frac{\sigma_0}{s^8} \frac{1 + z}{(1 - z)} 4 \ ,$$

where $z = \cos\theta_{cm}$, and $\sigma_0 = 440$ mb (GeV)^{14} as for the π^-p data. We notice that the measured cross-sections are higher than the predicted ones. The decrease

with energy, however, still seems to be faster than the predicted s^{-8} behaviour. This is further illustrated in Fig. 10 where the 90° c.m. differential cross-sections from different experiments[1,3,42,45,46,48,58-63] are plotted as a function of s. For comparison we also show corresponding data on K^+p elastic scattering. The straight lines correspond to s^{-16} (K^-p) and s^{-8} (K^+p). The parton model[38] predicts a ratio of the 90° c.m. K^+p and K^-p differential cross-sections of 16:1. This ratio has not been reached at our energy.

In the backward region the upper limit for the differential cross-section for $9.5 < -t < 10.5$ $(GeV/c)^2$, corresponding to $0 < -u < 1$ $(GeV/c)^2$, is 19 $nb/(GeV/c)^2$. Parametrizing the differential cross-section as $d\sigma/du = A \exp Bu$ and using the value of the slope in the backward direction found at 5 GeV/c [1], $B = 3.2$ $(GeV/c)^{-2}$, we obtain an upper limit for the differential cross-section at $u = 0$ of 73 $nb/(GeV/c)^2$. It is interesting to compare this value with the 5 GeV/c result $d\sigma/du\ (u = 0) = 350 \pm 160$ $nb/(GeV/c)^2$ [1]. The energy dependence of the cross-section parametrized as $d\sigma/du\ (u = 0) = \text{const} \times s^{-\alpha}$ corresponds to an exponent $\alpha = 9.8 \pm 0.4$ [1] for the range of incident momenta $1 < p_K < 3$ GeV/c. Between 5 and 6.2 GeV/c we obtain $\alpha > 7.8\ ^{+\ 2.0}_{-\ 3.1}$ still compatible with the lower energy result but significantly larger than the value $\alpha = 3$ calculated by Michael[53] considering exchange of Δ^{++} and K. We conclude that if double Regge exchange is to describe the backward peak at 5 GeV/c, more than one of the possible intermediate states have to be considered.

In Fig. 11 are plotted the differential cross-sections at $u = 0$ [1,45,64-66] as a function of the c.m. energy squared. The broken line is the prediction of Michael[53] for double Regge exchange. The full line represents a decrease as s^{-9}.

4. SUMMARY

Both the π^-p and K^-p elastic scattering cross-section data show dip-bump structures where the bump diminishes with increasing energy. At $-t \approx 1$ GeV/c there is a structure both for the π^-p and K^-p data, and it starts diminishing roughly at the same energy.

Using $\pi^\pm p$ data at 10 GeV/c as a normalization, the parton model[38] does not give good fits to the data in the energy range 5-10 GeV/c. As the domain of validity for parton models is confined to large values of s, t, and u, the disagreement may not be so surprising.

REFERENCES

1) Å. Eide, P. Lehmann, A. Lundby, C. Baglin, P. Briandet, P. Fleury, P.J. Carlson, E. Johansson, M. Davier, V. Gracco, R. Morand and D. Treille, Nuclear Phys. B60 (1973) 173.

2) C. Baglin, P. Briandet, P.J. Carlson, B. d'Almagne, Å. Eide, P. Fleury, V. Gracco, E. Johansson, P. Lehmann, A. Lundby, S. Mukhin, A. Navarro-Savoy, A. Pevsner, F. Richard, G. de Rosny, L. Staurset and D. Treille, Phys. Letters 47B (1973) 85.

3) C. Baglin, P. Briandet, P. Fleury, G. de Rosny, P.J. Carlson, K.E. Johansson, B. d'Almagne, P. Lehmann, M. Richard, D. Treille, Å. Eide, A. Lundby, A. Navarro-Savoy, L. Staurset and V. Gracco, Nuclear Phys. B98 (1975) 365.

4) C. Baglin, P. Briandet, P.J. Carlson, B. d'Almagne, Å. Eide, P. Fleury, V. Gracco, E. Johansson, P. Lehmann, A. Lundby, S. Mukhin, A. Navarro-Savoy, A. Pevsner, F. Richard, G. de Rosny, L. Staurset and D. Treille, Phys. Letters 47B (1973) 89.

5) T. Buran, Å. Eide, P. Helgaker, P. Lehmann, A. Lundby, A. Navarro-Savoy, L. Staurset, O. Sörum, C. Baglin, P. Briandet, P. Fleury, G. de Rosny, J.M. Thenard, P.J. Carlson, K.E. Johansson, B. d'Almagne, F. Richard, D. Treille and V. Gracco, Nuclear Phys. B97 (1975) 11.

6) K.J. Foley, S.J. Lindenbaum, W.A. Love, S. Ozaki, J.J. Russell and L.C.L. Yuan, Phys. Rev. Letters 11 (1963) 503.

7) K.J. Foley, R.S. Gilmore, S.J. Lindenbaum, W.A. Love, S. Ozaki, E.H. Willen, R. Yamada and L.C.L. Yuan, Phys. Rev. Letters 15 (1965) 45.

8) Fermilab Single-Arm Spectrometer Group, Phys. Rev. Letters 35 (1975) 1195.

9) C.W. Akerlof, R. Kotthaus, R.L. Loveless, D.I. Meyer, I. Ambats, W.T. Meyer, C.E.W. Ward, D.P. Eartly, R.A. Lundy, S.M. Pruss, D.D. Yovanovitch and D.R. Rust, Phys. Rev. Letters 35 (1975) 1406.

10) A.R. Dzierba, W.T. Ford, R. Gomez, P.J. Oddone, C.W. Peck, C. Rosenfeld, R.P. Ely and D.F. Grether, Phys. Rev. D 7 (1973) 725.

11) Yu.M. Antipov, C. Ascoli, R. Busnello, G. Damgaard, M.N. Kienzle-Focacci, W. Kienzle, R. Klanner, L.G. Landsberg, A.A. Lebedev, C. Lechanoine, P. Lecomte, M. Martin, V. Roinishvili, R.D. Sard, A. Weitsch and F.A. Yotch, Nuclear Phys. B57 (1973) 333.

12) A.A. Derevshchikov, Yu.A. Matulenko, A.P. Mecshanin, A.I. Mysnik, S.B. Nurushev, G.P. Proskurin, V.V. Siksin, E.V. Smirnov, L.F. Soloviev and V.L. Solovjanov, Nuclear Phys. B80 (1974) 442.

13) A.A. Derevshchikov, N.I. Golovin, Y.C. Khodirev, V.I. Kotov, S.B. Nurushev, Y.A. Matulenko, L.F. Soloviev, G.T. Adilov, F.K. Aleev, W. Gajewski, I. Ion, T.S. Nigmanov, B. Niczyporuk, E.N. Tsyganov, M. Turala, K. Wala, A.S. Vodopianov, E.B. Dally, D.J. Drickey, A.D. Liberman, P.F. Shepard and J.C. Tompkins, Phys. Letters 48B (1974) 367.

14) P.J. Duke, D.P. Jones, M.A.R. Kemp, P.G. Murphy, J.D. Prentice, J.J. Thresher and H.H. Atkinson, Phys. Rev. Letters 15 (1965) 468.

15) D.E. Damouth, L.W. Jones and M.L. Perl, Phys. Rev. Letters 11 (1963) 287.

16) C.T. Coffin, N. Dikmen, L. Ettlinger, D. Meyer, A. Saulys, K. Terwilliger and D. Williams, Phys. Rev. 159 (1967) 1169.

17) B.B. Brabson, R.R. Crittenden, R.M. Heinz, R.C. Kammerud, H.A. Neal, H.W. Paik and R.A. Sidwell, Phys. Rev. Letters 25 (1970) 553.

18) Aachen-Birmingham-Bonn-Hamburg-London (I.C.)-München Collaboration (L. Bondár et al.), Nuovo Cimento 31 (1964) 729.

19) M.L. Perl, Yong Yung Lee and E. Marquit, Phys. Rev. B138 (1965) 707.

20) P. Cornillon, G. Grindhammer, J.H. Klems, P.O. Mazur, J. Orear, J. Peoples, R. Rubinstein and W. Faissler, Phys. Rev. Letters 30 (1973) 403.

21) J. Orear, R. Rubinstein, D.B. Scarl, D.H. White, A.D. Krisch, W.R. Frisken, A.L. Read and H. Ruderman, Phys. Rev. 152 (1966) 1162.

22) D.P. Owen, F.C. Peterson, J. Orear, A.L. Read, D.G. Ryan, D.H. White, A. Ashmore, C.J.S. Damerell, W.R. Frisken and R. Rubinstein, Phys. Rev. 181 (1969) 1794.

23) A.A. Kartamyshev, K.N. Mukhin, A.S. Romantseva, M.M. Sulkovskaya and A.F. Sustavov, Phys. Letters 44B (1973) 310.

24) D. Harting, P. Blackall, B. Elsner, A.C. Helmholz, W.C. Middelkoop, B. Powell, B. Zacharov, P. Zanella, P. Dalpiaz, M.N. Focacci, S. Focardi, G. Giacomelli, L. Monari, J.A. Beaney, R.A. Donald, P. Mason, L.W. Jones and D.O. Caldwell, Nuovo Cimento 38 (1965) 60.

25) H. Brody, R. Lanza, R. Marshall, J. Niederer, W. Selove, M. Shochet and R. Van Berg, Phys. Rev. Letters 16 (1966) 828 and 968.

26) S.W. Kormanyos, A.D. Krisch, J.R. O'Fallon, K. Ruddick and L.G. Ratner, Phys. Rev. Letters 16 (1966) 709.

27) A.S. Carroll, J. Fischer, A. Lundby, R.H. Phillips, C.L. Wang, F. Lobkowicz, A.C. Melissinos, Y. Nagashima and S. Tewksbury, Phys. Rev. Letters 20 (1968) 607.

28) E.W. Hoffman, R.L. Dixon, J.M. Fletcher, A.F. Garfinkel, F.J. Loeffler, S. Mudrak, E.I. Shibata, K.C. Stanfield and Y.W. Tang, Phys. Rev. Letters 35 (1975) 138.

29) J. Banaigs, J. Berger, C. Bonnel, J. Duflo, L. Goldzahl, F. Plouin, W.F. Baker, P.J. Carlson, V. Chabaud and A. Lundby, Nuclear Phys. B8 (1968) 31.

30) W.F. Baker, P.J. Carlson, V. Chabaud, A. Lundby, J. Banaigs, J. Berger, C. Bonnel, J. Duflo, L. Goldzahl and F. Plouin, Nuclear Phys. B9 (1969) 249.

31) W.F. Baker, K. Berkelman, P.J. Carlson, G.P. Fisher, P. Fleury, D. Hartill, K. Kalbach, A. Lundby, S. Mukhin, R. Nierhaus, K.P. Pretzl and J. Woulds, Nuclear Phys. B25 (1971) 385.

32) R.J. Ott, J. Trischuk, J. Va'vra, T.J. Richards and L.S. Schroeder, Phys. Letters 42B (1972) 133.

33) A. Brabson, G. Calvelli, S. Cittolin, P. De Guio, F. Gasparini, S. Limentani, P. Mittner, M. Posocco, L. Ventura, C. Voci, M. Crozon, A. Diaczek, R. Sidwell and J. Tocqueville, Phys. Letters 42B (1972) 283.

34) R.R. Crittenden, K.F. Galloway, R.M. Heinz, H.A. Neal and R.A. Sidwell, Phys. Rev. D 1 (1970) 3050.

35) See, for example, V. Barger and R.J.N. Phillips, Phys. Rev. Letters 20 (1968) 564.

36) R.R. Crittenden, R.M. Heinz, D.B. Lichtenberg and E. Predazzi, Phys. Rev. D 1 (1970) 169.

37) V. Barger and D. Cline, Phys. Rev. 155 (1967) 1792.

38) J.F. Gunion, S.J. Brodsky and R. Blankenbecler, Phys. Rev. D 8 (1973) 287.

39) S.J. Brodsky and G.R. Farrar, Phys. Rev. Letters 31 (1973) 1153.

40) P.V. Landshoff, Phys. Rev. D 10 (1974) 1024.

41) See, for example, A.N. Diddens, Proc. 17th Internat. Conf. on High-Energy Physics, London, 1974 (Science Research Council, Rutherford Laboratory, Chilton, Didcot, England, 1974), p. I-41.

42) A.W. Lowman and N.A. McCubbin, Nuclear Phys. B61 (1973) 296.

43) R.J. Miller, J.J. Phelan, J.R. Smith, R. Barloutaud, C. Louedec, F. Pierre, J.P. Porte, M. Spiro, B. Drevillon, D. Linglin and R.A. Salmeron, Phys. Letters 34B (1971) 230.

44) J. Bartsch, M. Deutschmann, G. Kraus, M. Böttcher, U. Gensch, J. Kaltwasser, D. Pose, J.R. Campbell, V.T. Cocconi, J.D. Hansen, G. Kellner, W. Kittel, S. Matsumoto, D.R.O. Morrison, S. Stroynowski, J.B. Whittaker, N.C. Barford, G.A. Grammatikakis, B.R. Kumar, A.W. Mutalib, A. Frøhlich, P. Porth, P.Schmid and H. Wahl, Nuclear Phys. B29 (1971) 398.

45) M.N. Focacci, S. Focardi, G. Giacomelli, P. Serra, M.P. Zerbetto and L. Monari, Phys. Letters 19 (1965) 441.

46) J. Gordon, Phys. Letters 21 (1966) 117.

47) J. Banaigs, J. Berger, C. Bonnel, J. Duflo, L. Goldzahl, F. Plouin, W.F. Baker, P.J. Carlson, V. Chabaud and A. Lundby, Nuclear Phys. B9 (1969) 640.

48) Amsterdam-CERN-Nijmegen-Oxford Collaboration, Paper No G2-34 submitted to the EPS Internat. Conf. on High-Energy Physics, Palermo, 1975.

49) B. Drevillon, S. Borenstein, B. Chauraud, J.M. Gago, R.A. Salmeron, R. Barloutaud, A. Borg, M. Spiro, C. Wohl, C. Comber, K. Paler, S.N. Tovey and T.P. Shah, K^-p elastic scattering at 14.3 GeV/c, Paper No. G1-08 submitted to the EPS Internat. Conf. on High-Energy Physics, Palermo, 1975.

50) M. Aguilar-Benitez, R.L. Eisner and J.B. Kinson, Phys. Rev. D 4 (1971) 2583.

51) J. Mott, R. Ammar, R. Davis, W. Kropac, A. Cooper, M. Derrick, T. Fields, L. Hyman, J. Loken, F. Schweingruber and J. Simpson, Phys. Letters 23 (1966) 171.

52) C. Daum, F.C. Erné, J.P. Lagnaux, J.C. Sens, M. Steuer and F. Udo, Nuclear Phys. B6 (1968) 273.

53) C. Michael, Phys. Letters 29B (1969) 230.

54) J.S. Loos, U.E. Kruse and E.L. Goldwasser, Phys. Rev. 173 (1968) 1330.

55) I. Ambats, D.S. Ayres, R. Diebold, A.F. Greene, S.L. Kramer, A. Lesnik, D.R. Rust, C.E.W. Ward, A.B. Wicklund and D.D. Yovanovitch, Phys. Rev. D 9 (1974) 1179.

56) N.H. Buttimore and T.D. Spearman, Nuclear Phys. B84 (1975) 531, and private communication.

57) T. Lasinski, R. Levi-Setti, B. Schwarzschild and P. Ukleja, Nuclear Phys. B37 (1972) 1.

58) W. De Baere, J. Debaisieux, P. Dufour, F. Grard, J. Heughebaert, L. Pape, P. Peeters, F. Verbeure, R. Windmolders, R. George, Y. Goldschmidt-Clermont, V.P. Henri, B. Jongejans, D.W.G. Leith, A. Moisseev, F. Muller, J.M. Perreau and V. Yarba, Nuovo Cimento 45A (1966) 885.

59) M.G. Albrow, S. Andersson-Almehed, B. Bošnjaković, C. Daum, F.C. Erné, Y. Kimura, J.P. Lagnaux, F. Udo, J. Sens and F. Wagner, Nuclear Phys. B30 (1971) 273.

60) J. Whitmore, G.S. Abrams, L. Eisenstein, J. Kim, T.A. O'Halloran, Jr. and W. Shufeldt, Phys. Rev. D 3 (1971) 1092.

61) C.W. Akerlof, K.S. Han, D.I. Meyer, P. Schmueser, P.N. Kirk, D.R. Rust, C.E.W. Ward, D.D. Yovanovitch and S.M. Pruss, Phys. Rev. Letters 26 (1971) 1278.

62) J.N. MacNaughton, L. Feinstein, F. Marcelja and G. Trilling, Nuclear Phys. B14 (1969) 237.

63) J.A. Danysz, B.K. Penney, B.C. Stewart, G. Thompson, J.M. Brunet, J.L. Narjoux, J.E. Allen, N.J.D. Jacobs, D.H. Lewis and P.V. March, Nuclear Phys. B42 (1972) 29.

64) W.R. Holley, E.F. Beall, D. Keefe, L.T. Kerth, J.J. Thresher, C.L. Wang and W.A. Wenzel, Phys. Rev. 154 (1967) 1273.

65) P.J. Litchfield, T.C. Bacon, I. Butterworth, J.R. Smith, E. Lesquoy, R. Strub, A. Berthon, J. Vrana, J. Meyer, E. Pauli, B. Tallini and J. Zatz, Nuclear Phys. B30 (1971) 125.

66) A.S. Carroll, J. Fischer, A. Lundby, R.H. Phillips, C.L. Wang, F. Lobkowicz, A.C. Melissinos, Y. Nagashima, C.A. Smith and S. Tewksbury, Phys. Rev. Letters 23 (1969) 887.
Corrected data from C.A. Smith, Thesis (unpublished).

Table 1

Cross-section tables for π^-p elastic scattering at 6.21 GeV/c. Quoted errors are statistical. Systematic errors are estimated to ±20%.
$s = 12.556\ GeV^2$, $t + u = -10.756\ (GeV/c)^2$.

$-t$ $[(GeV/c)^2]$	Δt $[(GeV/c)^2]$	$\cos\theta_{cm}$	$d\sigma/dt$ $[\mu b/(GeV/c)^2]$	Error $[\mu b/(GeV/c)^2]$
0.35	0.1	+0.935	1292	51
0.45	0.1	+0.915	850	34
0.55	0.1	+0.897	425	22
0.65	0.1	+0.880	238	14
0.75	0.1	+0.860	130.9	8.5
0.85	0.1	+0.842	95.2	8.5
0.95	0.1	+0.825	66.3	6.3
1.05	0.1	+0.805	51.0	5.8
1.15	0.1	+0.787	30.6	4.6
1.25	0.1	+0.770	20.4	3.4
1.40	0.2	+0.740	15.5	2.3
1.60	0.2	+0.705	8.4	1.8
1.75	0.1	+0.676	6.30	0.29
1.85	0.1	+0.657	4.73	0.22
1.95	0.1	+0.638	3.80	0.19
2.05	0.1	+0.620	2.48	0.13
2.15	0.1	+0.602	1.55	0.093
2.25	0.1	+0.583	0.740	0.053
2.35	0.1	+0.564	0.440	0.038
2.45	0.1	+0.546	0.204	0.027
2.55	0.1	+0.528	0.099	0.020
2.65	0.1	+0.509	0.052	0.013
2.75	0.1	+0.490	0.045	0.013
2.85	0.1	+0.472	0.103	0.017
2.95	0.1	+0.453	0.109	0.020
3.05	0.1	+0.435	0.156	0.024
3.15	0.1	+0.417	0.208	0.029
3.25	0.1	+0.398	0.183	0.027
3.35	0.1	+0.379	0.181	0.029
3.45	0.1	+0.361	0.259	0.038
3.55	0.1	+0.342	0.172	0.027
3.65	0.1	+0.324	0.160	0.027
3.75	0.1	+0.305	0.178	0.033
3.85	0.1	+0.287	0.131	0.027

$-t$ $[(GeV/c)^2]$	Δt $[(GeV/c)^2]$	$\cos \theta_{cm}$	$d\sigma/dt$ $[\mu b/(GeV/c)^2]$	Error $[\mu b/(GeV/c)^2]$
3.95	0.1	+0.268	0.199	0.035
4.05	0.1	+0.250	0.105	0.024
4.15	0.1	+0.231	0.149	0.027
4.25	0.1	+0.213	0.102	0.022
4.35	0.1	+0.194	0.093	0.024
4.45	0.1	+0.176	0.080	0.022
4.60	0.2	+0.147	0.061	0.017
4.80	0.2	+0.111	0.062	0.022
5.10	0.4	+0.055	0.050	0.015
5.50	0.4	-0.019	0.0155	0.0095
5.90	0.4	-0.093	0.0232	0.0066
6.2	0.2	-0.149	0.0327	0.0088
6.4	0.2	-0.186	0.065	0.013
6.6	0.2	-0.222	0.066	0.013
6.8	0.2	-0.260	0.061	0.012
7.0	0.2	-0.297	0.0462	0.0095
7.2	0.2	-0.334	0.0411	0.0095
7.4	0.2	-0.371	0.0281	0.0069
7.6	0.2	-0.408	0.0376	0.0075
7.8	0.2	-0.445	0.0453	0.0082
7.95	0.1	-0.473	0.039	0.010
8.05	0.1	-0.492	0.040	0.012
8.15	0.1	-0.510	0.066	0.011
8.25	0.1	-0.528	0.063	0.013
8.35	0.1	-0.547	0.110	0.015
8.45	0.1	-0.566	0.091	0.013
8.55	0.1	-0.584	0.110	0.015
8.65	0.1	-0.602	0.180	0.019
8.75	0.1	-0.621	0.173	0.019
8.85	0.1	-0.640	0.200	0.020
8.95	0.1	-0.658	0.195	0.021
9.05	0.1	-0.676	0.296	0.027
9.15	0.1	-0.695	0.314	0.027
9.25	0.1	-0.714	0.294	0.027
9.35	0.1	-0.733	0.265	0.024
9.45	0.1	-0.751	0.270	0.024
9.85	0.7	-0.822	0.21	0.10
10.35	0.3	-0.915	0.48	0.24
10.60	0.2	-0.960	1.18	0.48

Table 2

Cross-section tables for K^-p elastic scattering at 6.21 GeV/c. Quoted errors are statistical. Systematic errors are estimated to ±20%.
$s = 12.814\ GeV^2$, $t + u = -10.566\ (GeV/c)^2$.

$-t$ $[(GeV/c)^2]$	Δt $[(GeV/c)^2]$	$\cos\theta_{cm}$	$d\sigma/dt$ $[\mu b/(GeV/c)^2]$	Error $[\mu b/(GeV/c)^2]$
0.31	0.02	+0.942	2096	58
0.33	0.02	+0.938	1812	50
0.35	0.02	+0.934	1549	44
0.37	0.02	+0.930	1228	35
0.39	0.02	+0.927	1114	33
0.41	0.02	+0.923	996	21
0.43	0.02	+0.919	831	18
0.45	0.02	+0.915	730	16
0.47	0.02	+0.912	648	15
0.49	0.02	+0.908	546	13
0.51	0.02	+0.904	472	11
0.53	0.02	+0.900	418	10
0.55	0.02	+0.897	351.8	8.9
0.57	0.02	+0.893	313.4	8.1
0.59	0.02	+0.889	261.1	6.9
0.61	0.02	+0.885	248.2	6.9
0.63	0.02	+0.881	207.8	6.0
0.65	0.02	+0.878	187.2	5.5
0.67	0.02	+0.875	171.3	5.2
0.69	0.02	+0.870	151.2	4.9
0.71	0.02	+0.865	139.0	4.6
0.73	0.02	+0.861	114.0	4.0
0.75	0.02	+0.858	108.9	3.8
0.77	0.02	+0.855	96.5	3.7
0.79	0.02	+0.851	88.2	3.5
0.81	0.02	+0.847	84.7	3.5
0.83	0.02	+0.845	73.4	3.1
0.86	0.04	+0.838	64.7	2.1
0.90	0.04	+0.830	58.1	2.0
0.94	0.04	+0.823	50.6	1.8
0.98	0.04	+0.815	46.4	1.8
1.02	0.04	+0.808	45.1	2.6
1.06	0.04	+0.800	38.7	2.3
1.10	0.04	+0.793	34.4	2.1

$-t$ $[(GeV/c)^2]$	Δt $[(GeV/c)^2]$	$\cos \theta_{cm}$	$d\sigma/dt$ $[\mu b/(GeV/c)^2]$	Error $[\mu b/(GeV/c)^2]$
1.14	0.04	+0.785	34.3	2.2
1.18	0.04	+0.778	29.9	2.0
1.25	0.10	+0.765	26.3	1.2
1.35	0.10	+0.745	23.1	1.1
1.45	0.10	+0.725	17.68	0.88
1.55	0.10	+0.705	14.33	0.77
1.70	0.20	+0.680	9.23	0.37
1.90	0.20	+0.640	5.56	0.27
2.10	0.20	+0.605	2.79	0.20
2.30	0.20	+0.565	1.630	0.087
2.50	0.20	+0.527	0.901	0.110
2.70	0.20	+0.490	0.379	0.085
2.90	0.20	+0.453	0.20	0.09
3.25	0.50	+0.385	0.089	0.056
3.75	0.50	+0.293	0.074	0.059
4.25	0.50	+0.197	0.028	$^{+0.038}_{-0.028}$
6.25	3.5	-0.18	0.014	$^{+0.006}_{-0.014}$
8.75	1.5	-0.65	0.022	$^{+0.007}_{-0.022}$
10.0	1.0	-0.89	0.019	$^{+0.010}_{-0.019}$

Table 3

Dip position [units for t and u are $(GeV/c)^2$]

6.2 GeV/c			5.0 GeV/c			Remarks
-t	-u	cos θ_{cm}	-t	-u	cos θ_{cm}	
2.8	8.1	+0.49	2.8	5.7	+0.33	Fixed t-dip (Fig. 2)
5.5	5.5	-0.02	4.7	3.8	-0.09	Fixed cos θ_{cm}? (Figs. 3,4)
7.4	3.6	-0.37	5.8	2.7	-0.33	Fixed cos θ_{cm}? (Figs. 3,4)
9.9	1.0	-0.83				Fixed u-dip (Fig. 5)

Figure captions

Fig. 1 : Layout for the 6.2 GeV/c experiment: S_1-S_4 are scintillation counters; C_1-C_3 are beam Čerenkov counters; T_1, T_3, and T_4 are trigger counters; W_1-W_4 are spark chamber telescopes; V_1-V_3 are veto counters; CW_3 is a Čerenkov counter.

Fig. 2 : The differential cross-section of π^-p scattering as a function of t. Comparison of our data at 6.2 GeV/c with the data of Eide et al. at 5.0 GeV/c (Ref. 1) and Owen et al. (Ref. 22) at 9.7-9.8 GeV/c.

Fig. 3 : The differential cross-section of π^-p scattering as a function of $\cos\theta_{cm}$. Comparison of our data at 6.2 GeV/c with data of Eide et al. at 5.0 GeV/c (Ref. 1) and Owen et al. (Ref. 22) at 9.7-9.8 GeV/c. The curves are prediction of a parton model of Gunion (Ref. 38) at the same three energies.

Fig. 4 : The differential cross-section of π^-p scattering as a function of $\cos\theta_{cm}$ in the large angular region. Comparison of our data at 6.2 GeV/c with the data of Eide et al. at 5.0 GeV/c (Ref. 1) and Owen et al. (Ref. 22) at 9.7-9.8 GeV/c.

Fig. 5 : The differential cross-section of π^-p scattering as a function of u. Comparison of our data at 6.2 GeV/c (filled circles) with the data of Banaigs et al. (Ref. 29), Baker et al. (Ref. 30), and Coffin et al. (Ref. 16) at 3.5 GeV/c, with Eide et al. (Ref. 1) $\left[-u > 1\ (GeV/c)^2\right]$ and Hoffman et al. (Ref. 28) $\left[-u < 1\ (GeV/c)^2\right]$ at 5.0 GeV/c, and with Owen et al. at 9.7-9.8 GeV/c (Ref. 22). Our data for small values of -u are from target 1.

Fig. 6 : The differential cross-sections of K^-p elastic scattering in the forward direction as a function of t. Comparison of our data at 6.2 GeV/c (filled circles) with the data of Ambats et al. (Ref. 55) at 6.0 GeV/c (open circles).

Fig. 7 : The slope b for the relation $d\sigma/dt = A\, e^{bt}$ fitted to the data points. Each point on the plot represents a different set of data points. All sets start with the lowest t-value, namely $-t = 0.31\ (GeV/c)^2$. The b-values displayed are placed at the maximum t-value for the data points used for the fit. Filled circles, this experiment, and open triangles, Ref. 42. Also shown are the χ^2 probabilities obtained in our fit (open circles, right scale).

Fig. 8 : The differential cross-section of K^-p elastic scattering as a function of t. The 3.59 GeV/c data are from Ref. 42, the 5 GeV/c data from Ref. 1, and the 10.1 GeV/c data from Ref. 44.

Fig. 9 : The differential cross-sections of K^-p elastic scattering as a function of $\cos \theta_{cm}$. The 3.59 GeV/c data are from Ref. 42, the 5 GeV/c data from Ref. 1, and the 6.2 GeV/c data are from this experiment. The curve is a prediction of the parton model for 6.2 GeV/c discussed in the text.

Fig. 10 : The differential cross-section at $\cos \theta_{cm} = 0$ for $K^{\pm}p$ elastic scattering is shown as a function of the centre-of-mass energy squared s. The corresponding lab. momentum is also shown. The full lines are fits to the data to the form $d\sigma/dt = \text{const} \times s^{-\alpha}$. For K^-p we get $\alpha = 16.3 \pm 1.1$ (full line) and for K^+p $\alpha = 9.5 \pm 0.6$ (broken line). The data are from Refs. 1, 42, 46, 47, 49 and from this experiment (K^-p) and from Refs. 1, 3, 58, 59, 60 and 66 (K^+p).

Fig. 11 : The energy dependence of the differential cross-section for K^-p elastic scattering at $u = 0$. The straight line has the energy dependence $d\sigma/du = \text{const} \times s^{-9}$. The broken line corresponds to $d\sigma/du = 8.1\ p_{lab}^{-3}\ \mu b/(GeV/c)^2$, an estimate of double Regge exchange given by Michael (Ref. 53). Data from Refs. 1, 45 and 64-66.

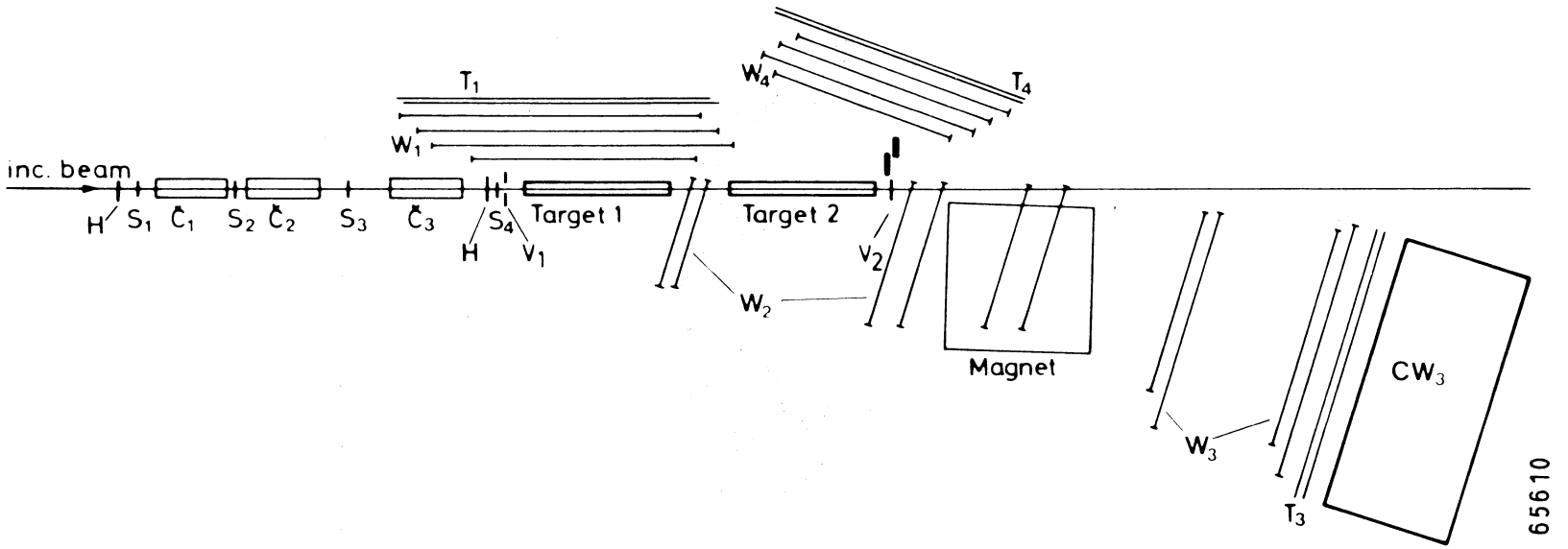
T1
W4
T4
W1
inc. beam
H
S1
C1
S2
C2
S3
C3
S4
Target 1
Target 2
H
V1
V2
W2
Magnet
W3
CW3
T3
65610

Fig. 1

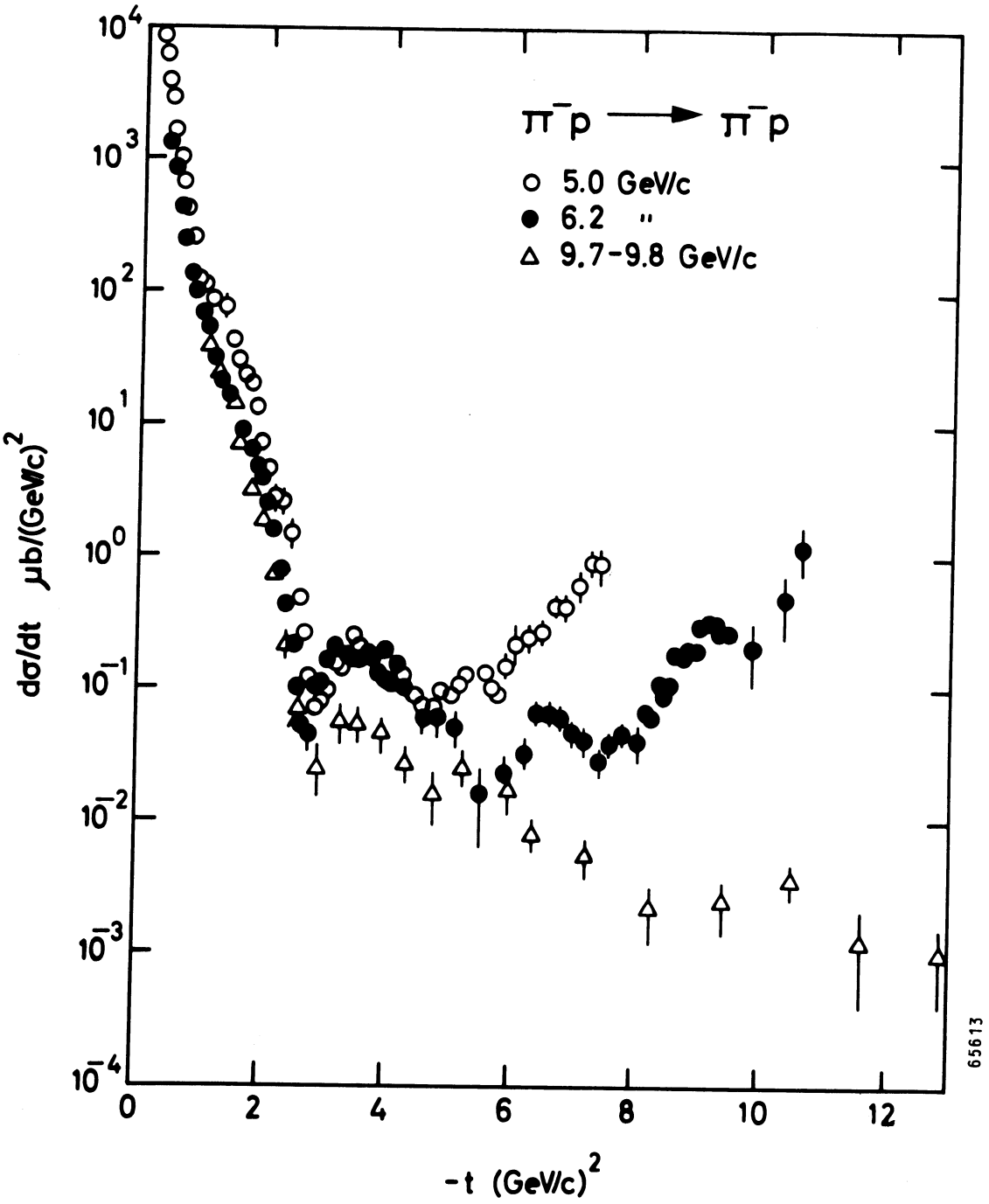
$\pi^- p \longrightarrow \pi^- p$
5.0 GeV/c
6.2 "
9.7-9.8 GeV/c
$d\sigma/dt$ $\mu b/(GeV/c)^2$
$-t$ $(GeV/c)^2$
65613

Fig. 2

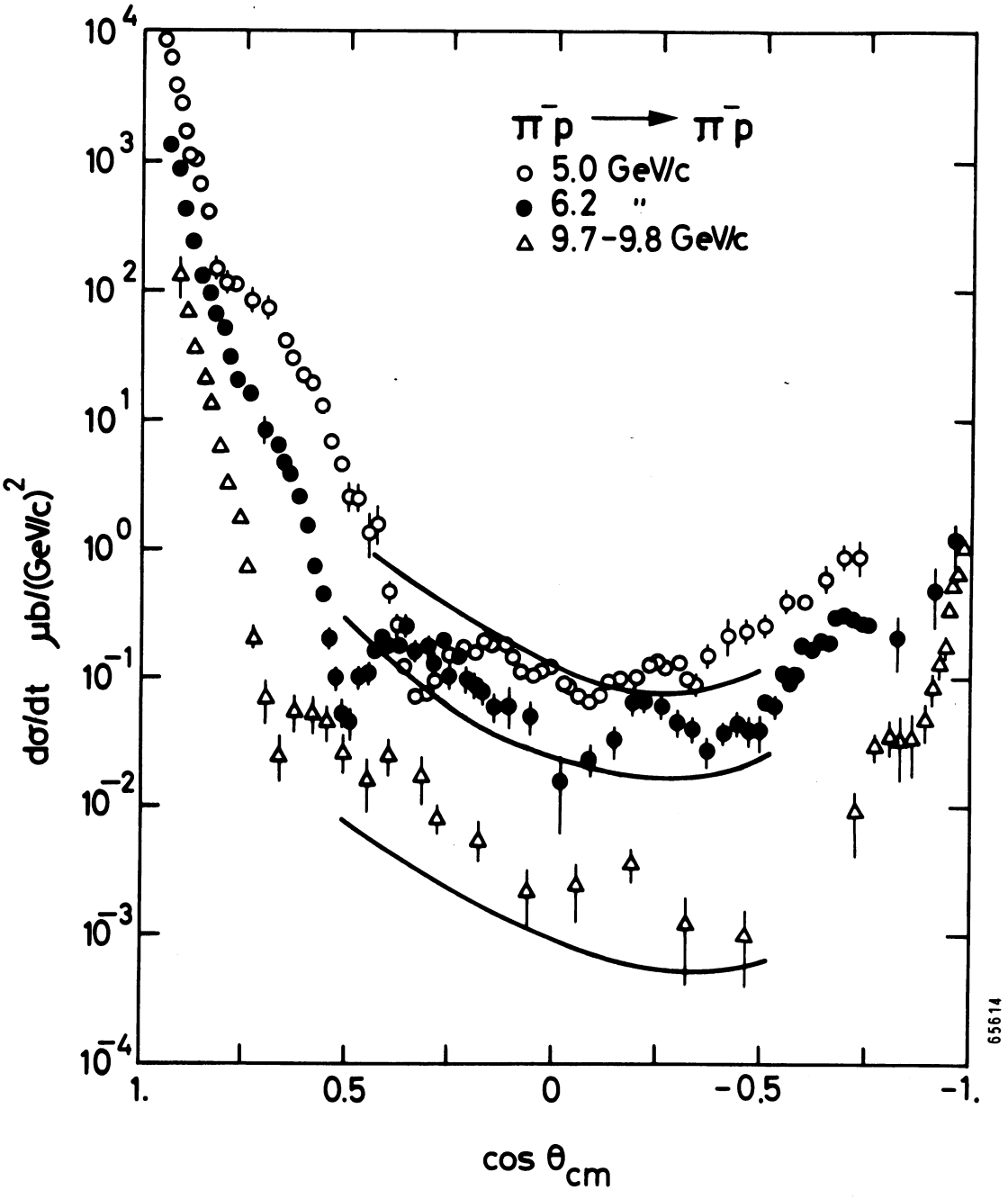
$\pi^- p \longrightarrow \pi^- p$
5.0 GeV/c
6.2 "
9.7-9.8 GeV/c
$d\sigma/dt$ $\mu b/(GeV/c)^2$
10^4
10^3
10^2
10^1
10^0
10^{-1}
10^{-2}
10^{-3}
10^{-4}
1.
0.5
0
-0.5
-1.
$\cos \theta_{cm}$
65614

Fig. 3

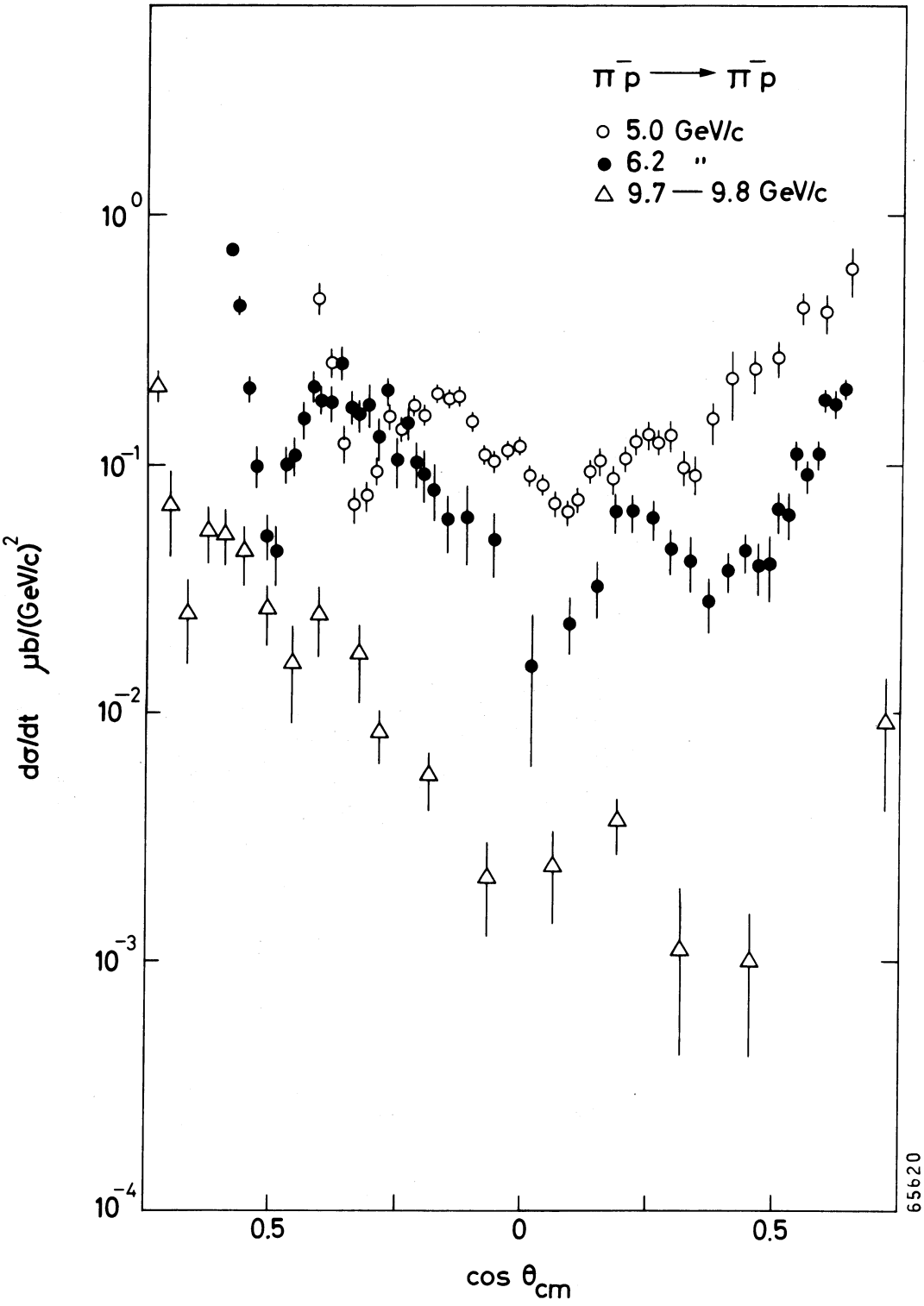
$\pi^- p \longrightarrow \pi^- p$
○ 5.0 GeV/c
● 6.2 "
△ 9.7 — 9.8 GeV/c
10^0
10^{-1}
10^{-2}
10^{-3}
10^{-4}
$d\sigma/dt$ μb/(GeV/c)^2
0.5
0
0.5
cos θ_{cm}
65620

Fig. 4

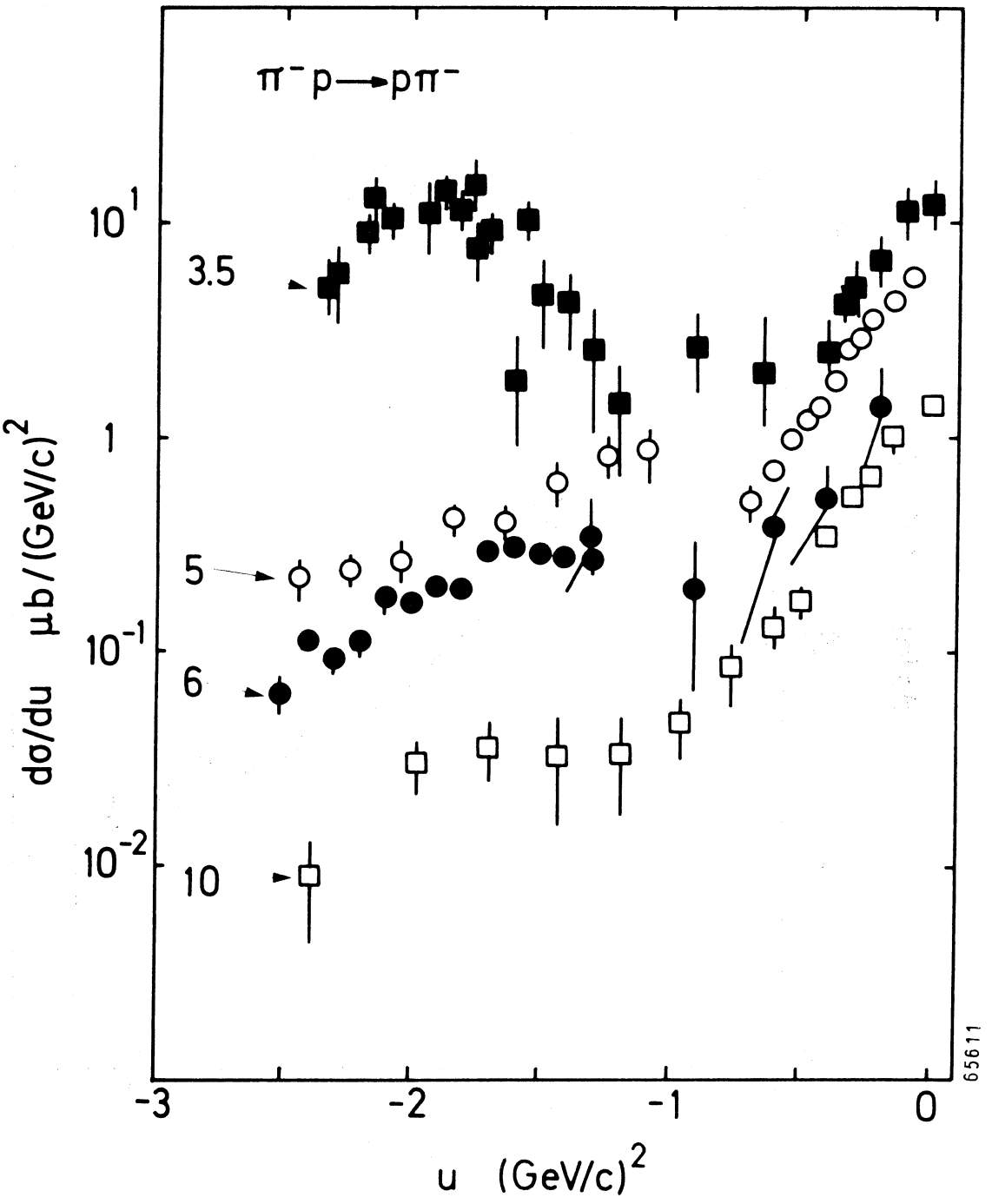
$\pi^- p \rightarrow p\pi^-$
10^1
1
10^{-1}
10^{-2}
3.5
5
6
10
$d\sigma/du$ μb/(GeV/c)^2
-3
-2
-1
0
u (GeV/c)^2
65611

Fig. 5

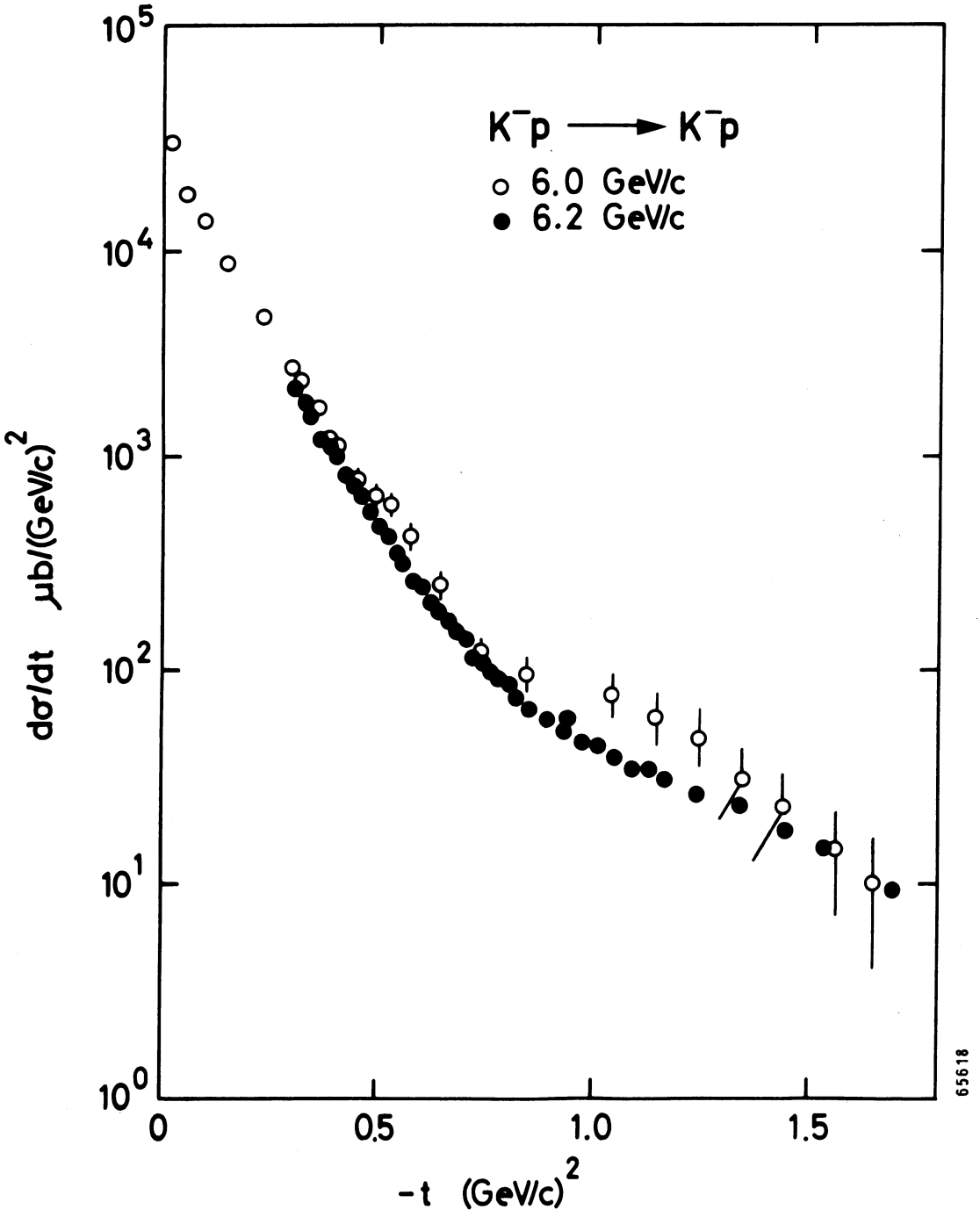
$K^-p \longrightarrow K^-p$
6.0 GeV/c
6.2 GeV/c
$d\sigma/dt$ $\mu b/(GeV/c)^2$
10^5
10^4
10^3
10^2
10^1
10^0
0
0.5
1.0
1.5
$-t$ $(GeV/c)^2$
65618

Fig. 6

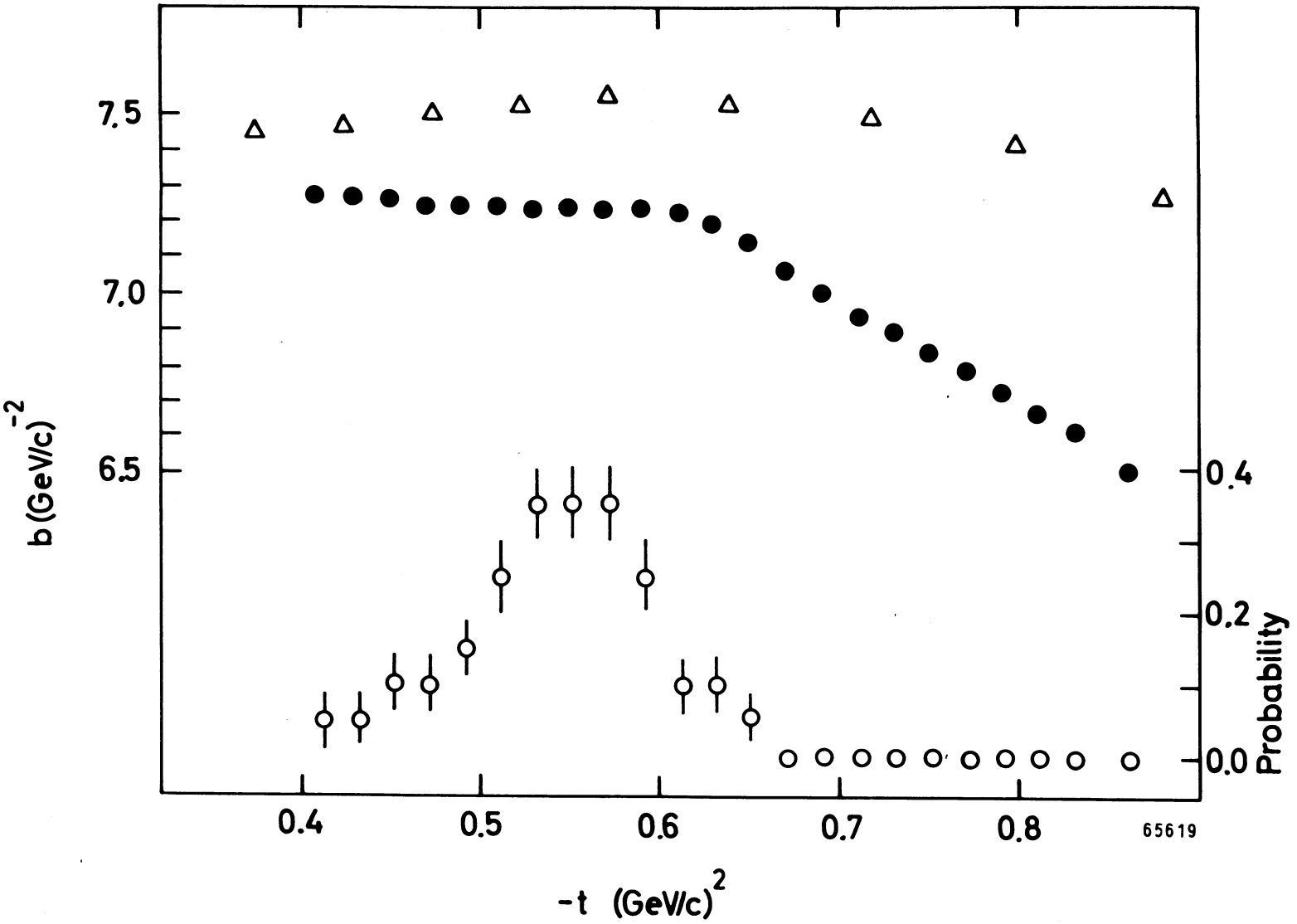
7.5
7.0
6.5
b (GeV/c)$^{-2}$
0.4
0.2
0.0
Probability
0.4
0.5
0.6
0.7
0.8
65619
-t (GeV/c)^2

Fig. 7

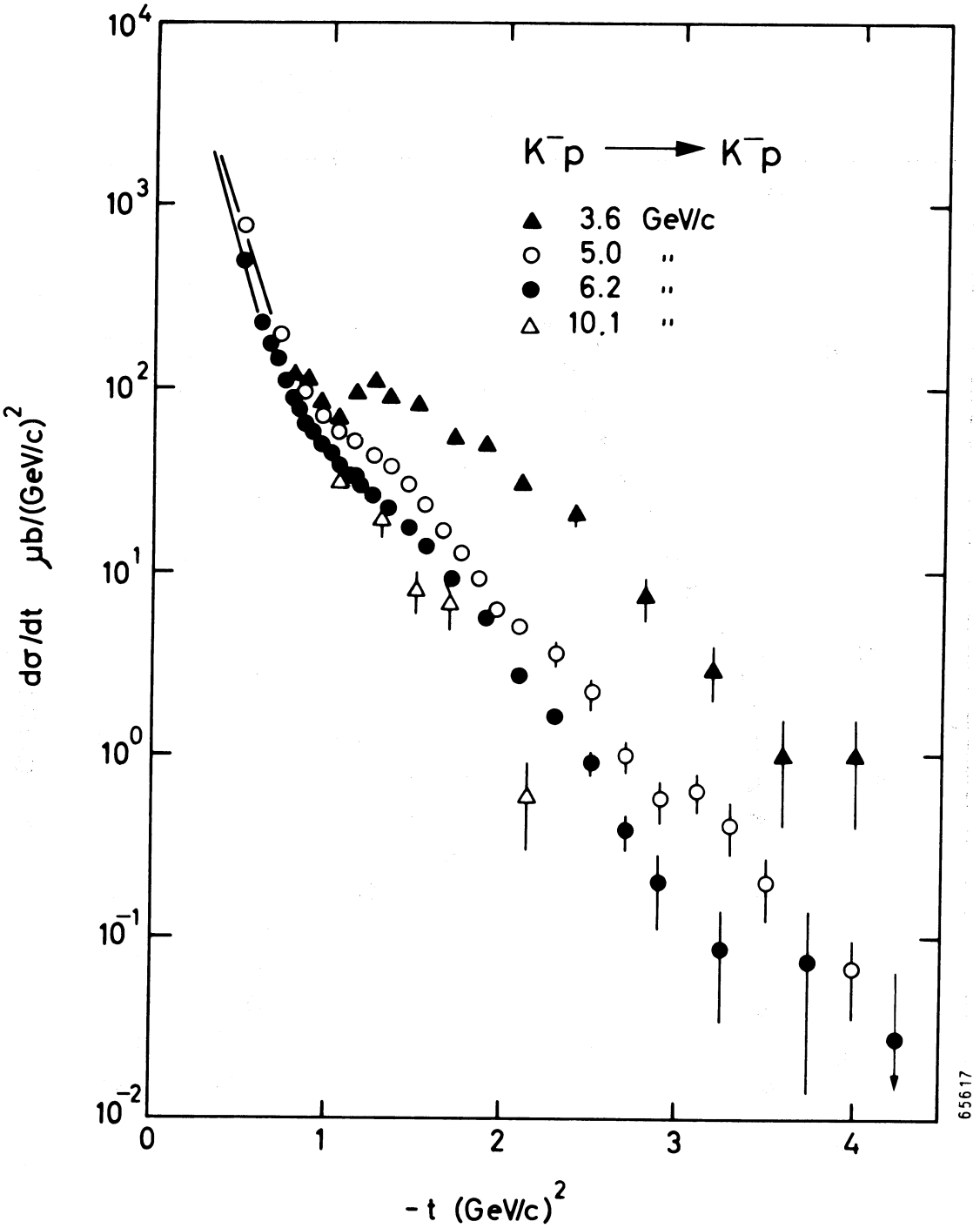
$K^-p \longrightarrow K^-p$
3.6 GeV/c
5.0 "
6.2 "
10.1 "
$d\sigma/dt$ $\mu b/(GeV/c)^2$
$-t\ (GeV/c)^2$
65617

Fig. 8

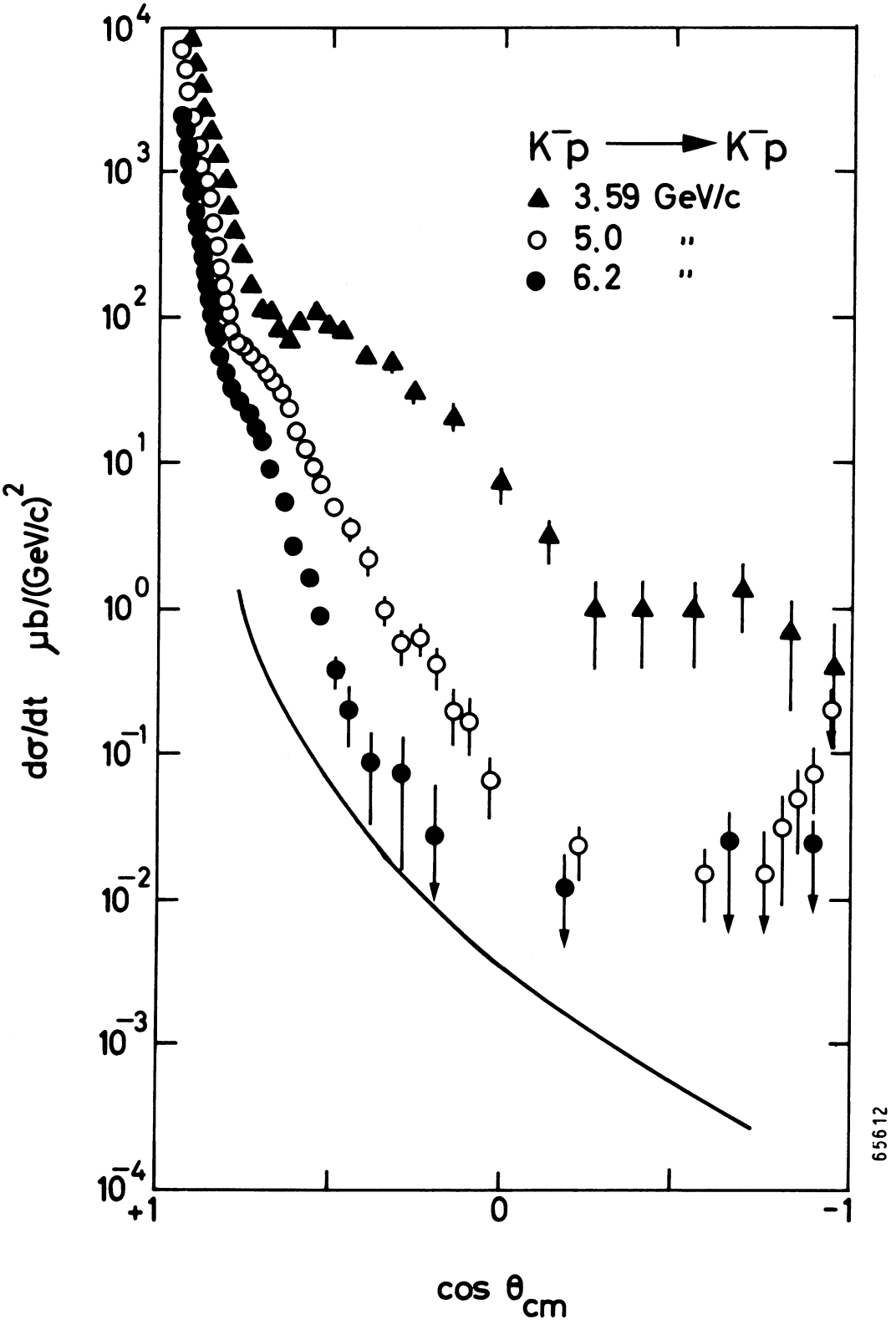
$K^-p \longrightarrow K^-p$
▲ 3.59 GeV/c
○ 5.0 "
● 6.2 "
$d\sigma/dt$ μb/(GeV/c)^2
10^4
10^3
10^2
10^1
10^0
10^{-1}
10^{-2}
10^{-3}
10^{-4}
+1
0
-1
cos θ_{cm}
65612

Fig. 9

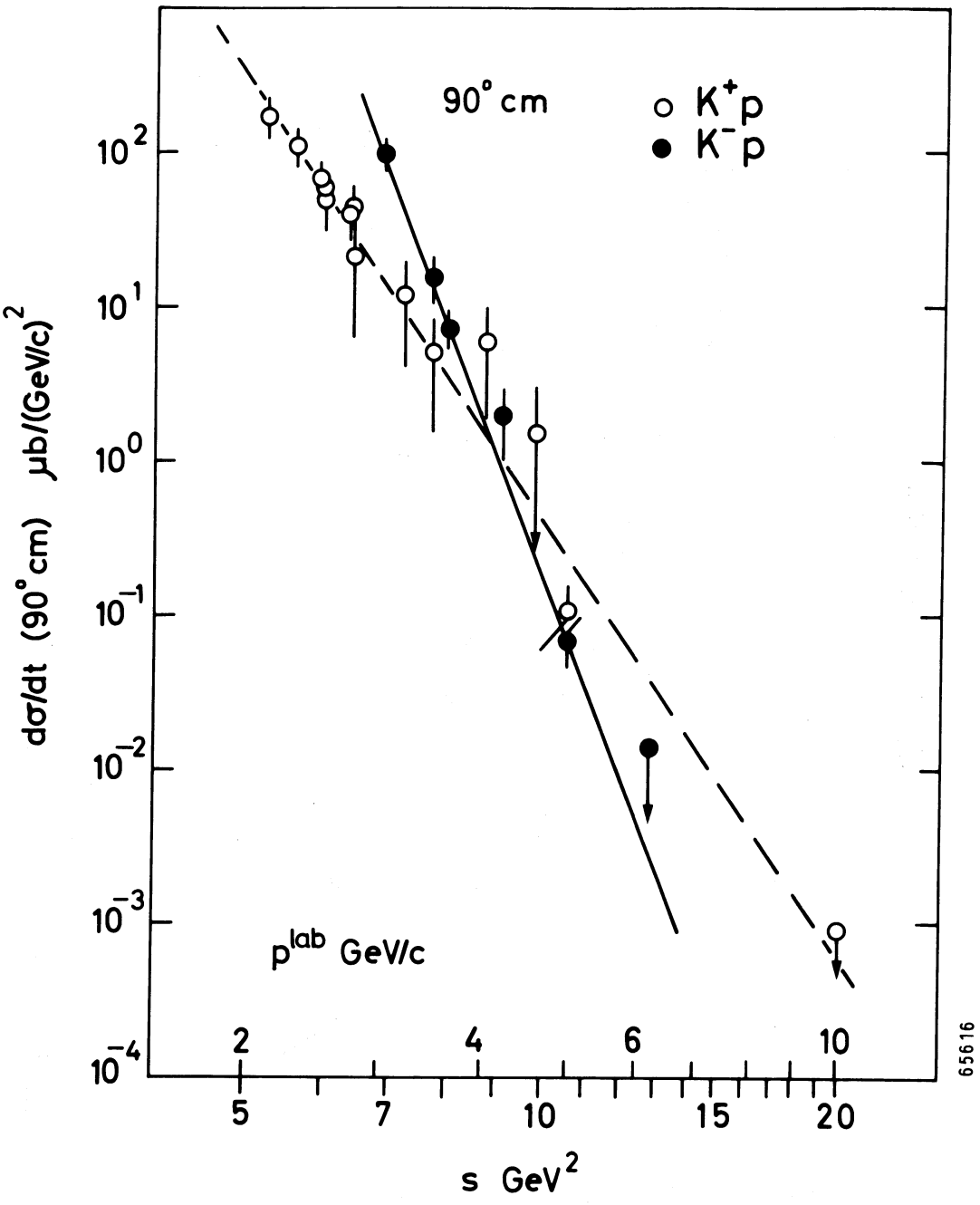
90° cm
K+p
K−p
dσ/dt (90°cm) μb/(GeV/c)2
10^2
10^1
10^0
10^-1
10^-2
10^-3
10^-4
plab GeV/c
2
4
6
10
5
7
10
15
20
s GeV2
65616

Fig. 10

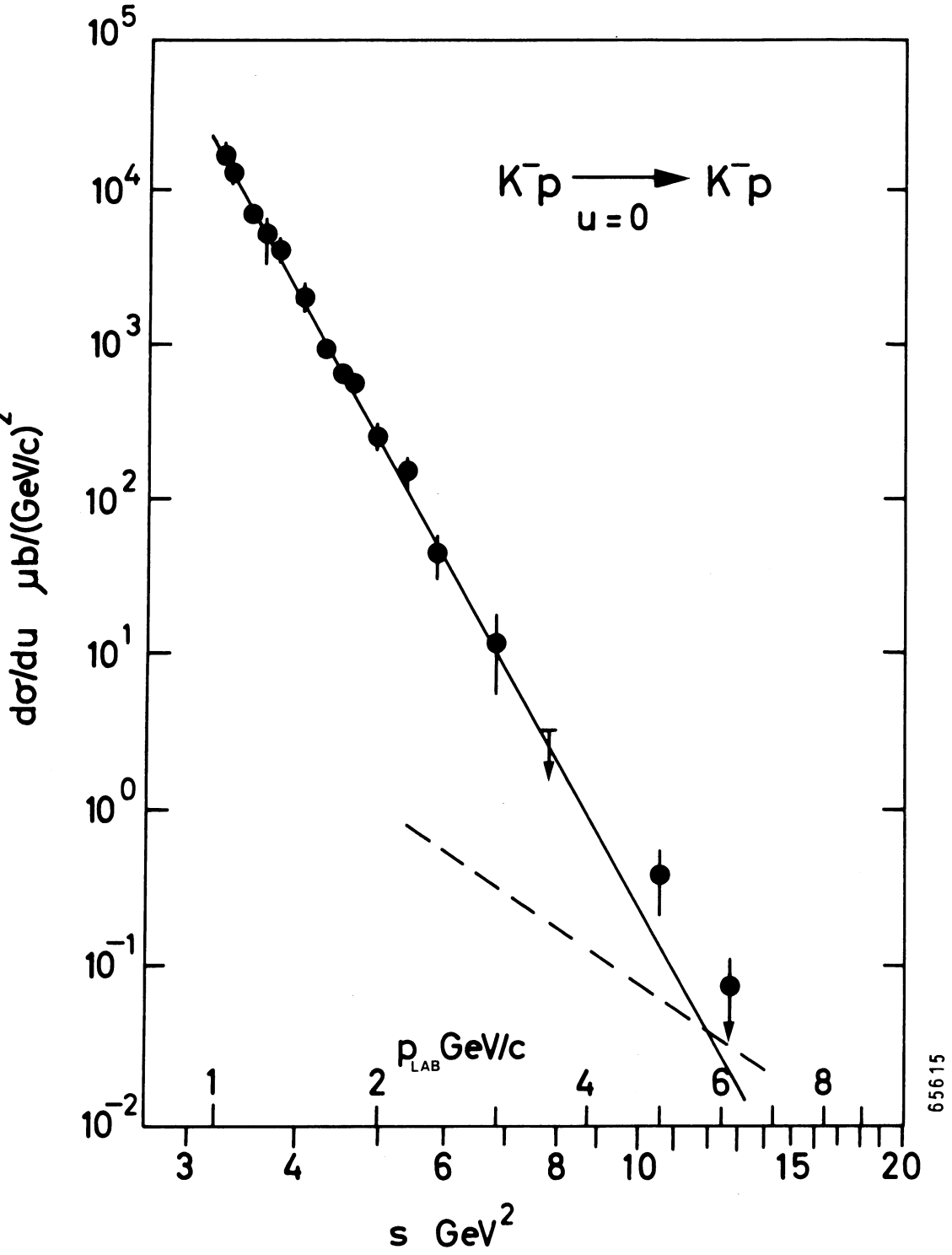
$K^-p \rightarrow K^-p$
u = 0
$d\sigma/du\ \mu b/(GeV/c)^2$
p_{LAB} GeV/c
s GeV^2
65615

Fig. 11